Interface roughness governed negative magnetoresistances in two-dimensional electron gases in AlGaN/GaN heterostructures

Ting-Ting Wang[1], Sining Dong[1], Zhi-Li Xiao[2,3,*], Chong Li[1], Wen-Cheng Yue[1], Bin-Xi Liang[1], Fei-Fan Xu[1], Yong-Lei Wang[1,*], Sheng-Rui Xu[4], Xiao-Li Lu[4,*], Jianhua Li[1], Chenguang Wang[1], Zixiong Yuan[1], Song-Lin Li[1], Guo-Zhu Sun[1,5], Bin Liu[1], Hai Lu[1], Hua-Bing Wang[1,5], and Wai-Kwong Kwok[2]

[1]*School of Electronic Science and Engineering, Nanjing University, Nanjing, 210023, China*

[2]*Materials Science Division, Argonne National Laboratory, Argonne, IL 60439, USA*

[3]*Department of Physics, Northern Illinois University, DeKalb, IL 60115, USA*

[4]*School of Microelectronics & State Key Discipline Laboratory of Wide Bandgap Semiconductor Technology, Xidian University, Xi'an, 710071, China*

[5]*Purple Mountain Laboratories, Nanjing, 211111, China*

Negative magnetoresistances (NMRs) have been widely observed in two-dimensional electron gases (2DEGs). However, their origins are under debate. Here, we report on NMRs in the 2DEG in AlGaN/GaN heterostructures, aiming to uncover their origins by utilizing electric field gating. We systematically measured the magnetoresistances in magnetic fields up to 12 T and at temperatures between 3 K and 260 K and observed NMRs over a wide range of temperatures from 3 K to 170 K, which become more pronounced with decreasing temperature. We conducted electric field gating experiments to correlate the occurrence of NMRs with the relationship between electron mobility and density. The latter is governed by defect scattering sources in the sample and can be theoretically modelled. Comparison of the measured electron mobility and electron density relationship with theory reveals that interface roughness scattering plays a crucial role in obtaining large NMRs. Our work demonstrates that electric field gating provides a means not only to tune the values of NMRs but also to uncover their mechanisms.

I. INTRODUCTION

Negative magnetoresistances (NMR), where the magnetic field induces a decrease in the electrical resistance, is ubiquitous in two-dimensional electron gases (2DEGs) formed at the interfaces of various semiconductor heterostructures [1-23]. A common mechanism that can cause NMRs in 2DEGs is the weak localization (WL) of noninteracting electrons due to quantum interference effect [13-15,17-21]. The WL-induced NMRs only occur at low temperatures and at low magnetic fields, i.e., $\omega_c\tau < 1$ with ω_c being the cyclotron frequency and τ being the relaxation time. Their amplitudes are typically small (< -1%) and saturate quickly with increasing magnetic field. They also exhibit characteristic cusps at zero field in the resistance versus magnetic field $R(B)$ curves and therefore can be identified without difficulties. On the other hand, NMRs in some 2DEGs can be as large as -92% [8] and persist up to very high magnetic fields where $\omega_c\tau >> 1$ [19,22]. Various theories have been proposed to explain the underlying mechanisms that could lead to those large NMRs [24-31]. To date, the variety of non-WL NMRs observed in 2DEGs has been mostly attributed to electron–electron interaction (EEI) effect [1,2,24-26], Lorentz gas model [11,12,27,28], and memory effects resulting from the return events of an electron to a scatterer after a single collision process with another scatterer [19,29]. Recently, a theory [31] based on viscous flows of electrons could reproduce the colossal NMRs observed in 2DEGs in AlGaAs/GaAs hetereostructures [8]. Besides a few experiments that are particularly designed to prove theoretical predictions [11,12], in many cases, the behavior of the temperature and field dependence of the magnetoresistance is used to reveal a proposed mechanism [1,2,19]. Conclusions attained this way can be indecisive, since similar NMR behaviors can originate from

different mechanisms. For example, NMRs originating from both EEI [2,26] and memory effects [29] exhibit parabolic magnetic field dependence. Furthermore, the observed NMRs may be a result of several combined mechanisms, thereby complicating the analysis of the experimental data [19]. Here, we show that additional information on the origins of NMRs in 2DEGs can be obtained by electric field gating investigations of the electron mobility versus density relationship that can directly reflect the scattering sources in the sample [32-35].

AlGaN/GaN heterostructures have attracted extensive attention over the past years because they are well suited for fabricating high power and high frequency field effect transistors [36-38]. Good device performances hinge on the combination of their high carrier density and high breakdown fields [38]. The spontaneous and strong piezoelectric polarization in AlGaN/GaN heterostructures [39-41] creates a triangular quantum well resulting in 2DEGs with densities reaching values of ~10^{13} cm^{-2}, which is nearly two orders of magnitude larger than the typical densities (~10^{11} cm^{-2}) of 2DEGs in AlGaAs/GaAs systems [6-8]. Here we do not study other remarkable properties of the AlGaN/GaN heterostructure but focus on the origin of NMRs by taking advantage of the well-established relationship between the scattering sources and the density dependence of the electron mobility. The mobilities of the 2DEGs in AlGaN/GaN heterostructures are very limited (up to 10^4 $cm^2V^{-1}s^{-1}$). Thus, their mean free paths (see Fig.S1(b)) can be much smaller than the sample width, excluding mechanisms such as viscous flows [31] for the observed NMRs. The relationship between the scattering sources and the density dependence of the electron mobility, which can be obtained via electric field gating, has been extensively investigated both experimentally [32,33] and theoretically [see supplement]. That is, the scattering

source(s) causing the NMRs can be directly uncovered from the density dependence of the electron mobility. Here, we conduct a systematic investigation of electric field gating effect on the NMRs 2DEGs in AlGaN/GaN heterostructures to identify the regime where NMRs are observed in the density dependence of the electron mobility, revealing the crucial role played by the interface roughness [42,43] on the occurrence of large NMRs. This work demonstrates that electric field gating provides a means not only to tune the values of NMRs but also to uncover their mechanisms. It also indicates that magnetotransport can be used to characterize large-angle interface roughness scattering in AlGaN/GaN heterostructures.

II. EXPERIMENTAL METHODS

The AlGaN/GaN heterostructures investigated in this work were grown by metal-organic chemical vapor deposition (MOCVD) on sapphire substrates. Their layer structure is illustrated by the schematic presented in Fig.1(a). An AlN barrier layer was added between the AlGaN layer and the GaN buffer to reduce the alloy disorder scattering by minimizing the wave function penetration from the 2DEG channel into the AlGaN layer [44]. The 2DEG is realized due to spontaneous and piezoelectric polarizations in the GaN layer near the GaN/AlN interface. The measured samples were fabricated from the AlGaN/GaN heterostructure into a Hall bar geometry using photolithography, followed by inductively coupled plasma (ICP) etching. Ohmic contacts of Ti(20nm)/Al(120nm)/Ni(50nm)/Au(100 nm) were made by means of electron-beam evaporation (EBE), followed with a 30 s rapid thermal annealing at 850°C. Lastly, the gate electrode comprised of Ti(20 nm)/Au(100 nm) was made by means of EBE. Micrographs of a typical sample (Sample

W1) are presented in Fig.1(b).

We conducted conventional resistance measurements in an Oxford Instrument system (TeslatronPT) under constant current mode. Magnetic fields up to 12 Tesla were applied out-of-plane, i.e., perpendicular to the plane of the 2DEG. We define the magnetoresistance, i.e., the magnetic-field induced change of the resistance as $\gamma_{\mathrm{MR}} = (R - R_0)/R_0$, where R and R_0 are resistances at a fixed temperature with and without an applied magnetic field, respectively. We measured two samples (Sample W1 and Sample W2). Each of them has two sets of voltage contacts of neighboring sections (denoted as CH1 and CH2 in Fig.1(b) for Sample W1). Results from both CH1 and CH2 are nearly the same (see Fig.S1) [45]. We present results from CH1 of Sample W1 in the main text. Data from CH2 of Sample W1 and Sample W2 are presented in the supplement (see Fig.S1, Fig.S2 and Fig.S4) [45].

III. RESULTS AND DISCUSSION

Inset of Fig.1(c) exhibits $R_{xy}(B)$ curves obtained at the lowest (T = 3 K) and highest (T = 260 K) experimental temperatures. They indicate that the amplitude of the Hall resistances increases monotonically with increasing magnetic field and the slopes of $R_{xy}(B)$ curves are nearly independent of the temperature, which is the classical characteristic of Hall resistances for one type of charge carriers with a density that is temperature-insensitive. The slopes of the $R_{xy}(B)$ curves at various temperatures or the $R_{xy}(T)$ curve at a fixed magnetic field enables us to obtain the electron density. We measured $R_{xy}(T)$ at B = 9 T (see upper curve in Fig.1(c)) and obtained the temperature dependence of the electron density $n(T)$ as shown in Fig.1(d). The electron density is

nearly temperature-independent, with values of 1.02×10^{13}/cm^2 at T = 3 K and 1.12×10^{13}/cm^2 at T = 260 K, consistent with calculated values based on spontaneous and strain-induced polarization at the GaN/AlN interface [23,32,33]. Using the derived $n(T)$ and the measured zero-field $R_0(T)$ curves in Fig.1(c) we calculated the temperature dependence of the electron mobility $\mu(T)$ and present it in Fig.1(d). The Hall mobility is μ = 8000 cm^{2}V^{-1}s^{-1} at T = 3 K and decreases slowly with temperature up to 100 K, then it decreases more rapidly down to μ = 2000 cm^{2}V^{-1}s^{-1} at 260 K, mainly due to strong optical phonon scattering which is dominant in the high temperature region [46]. Compared to the electron mobility of 2DEGs in AlGaAs/GaAs heterostructures [7,8] where $\mu \sim 10^6$-10^7 cm^{2}V^{-1}s^{-1}, our observed value is relatively low but typical for AlGaN/GaN heterostructures [32,33,47].

Figure 2(a) shows $MR(B)$ curves obtained in magnetic fields of -12 T ≤ B ≤ +12 T and at T = 3K. At very low magnetic fields (inset of Fig.2(a)), the longitudinal resistance behavior shows a rapid decrease that can be attributed to WLs, typically observed in disordered semiconductor systems [15,16]. The *MR*s show a negative parabolic magnetoresistance in the range of intermediate magnetic fields as demonstrated by the inset of Fig.2(b). In higher magnetic fields, Shubnikov de Haas (SdH) quantum oscillations [19] are observed. Concurrently, at the fields where SdH oscillations emerge, the *MR* deviates from a parabolic magnetic field dependence (see Fig.2(b)). It is worth noting that the WL-induced *MR*s and SdH oscillations occur only at low temperatures and both effects gradually weaken and disappear with the increase of temperature. Meanwhile, the magnitude of the NMRs decreases gradually with increasing temperature, and eventually positive *MR*s emerge at high temperatures (see Fig.2(c); more data are shown in

Fig.S2(a)). Similar results are obtained in CH2 of Sample W1 (Fig.S2(b)) and Sample W2.

Besides weak localizations that induce small NMRs at very weak fields with a cusp at zero field, various other mechanisms based on both quantum [24-26,31] and quasiclassical [27-29] origins have been proposed to account for the large NMRs that occur at higher magnetic fields. For example, electron–electron interactions (EEIs) were considered in understanding the NMRs in high mobility [(0.42-5.5)×10^5 $cm^2V^{-1}s^{-1}$] 2DEGs in AlGaAs/GaAs heterostructures [1,2]. The EEIs lead to a parabolic negative magnetoresistance at $\omega_c\tau > 1$ [Refs.2,26]:

$$\gamma_{\mathrm{MR}} = -\frac{(\omega_c\tau)^2}{\pi k_F l} G_F(k_B T\tau/\hbar) \qquad (1)$$

where $\omega_c = eB/m^*$ is the cyclotron frequency and m^* is the effective mass, k_F is the Fermi wave number and l is the mean free path. The function $G_F(x)$ has the asymptotes $G_F(x \ll 1) \approx \mathrm{const} - lnx$ and $G_F(x > 1) \approx (c_0/2)x^{-1/2}$, with $c_0 \approx 0.276$. Clearly, Eq.1 correctly describes the parabolic behavior in the magnetic field dependence of the observed NMRs, as presented in Fig.2(b), where $B > 1.25$ T satisfies the requirement of $\omega_c\tau > 1$ at $\mu = 8000$ $cm^2V^{-1}s^{-1}$. Qualitatively, Eq.1 can also account for the decrease of the NMR's amplitude with increasing temperature, as shown in Fig.2(c).

However, the derived experimental G_F varies with $k_B T\tau/\hbar$ much slower than that predicted from theory (see Fig.S3(a)). More importantly, an essential feature of the EEI theory is that the impurities are treated as smooth random potential (remote impurities). This condition is satisfied in high-mobility GaAs structures, where doping impurities are separated from the 2DEGs by an undoped spacer and the scattering potential has a long-range character [2]. However, in

AlGaN/GaN heterostructures, a random array of strong scatterers (such as interface roughness) that give rise to predominantly large angle scattering can exist and contribute to the occurrence of large NMRs [19].

In the presence of strong scatterers, the Lorentz-Boltzmann quasiclassical model predicts that a fraction *P* of the electrons in the 2DEG system remains eternally in collisionless cyclotron orbits around the scatterers. Such orbiting electrons do not contribute to the conductivity σ_{xx}; however, they give a nonzero contribution to σ_{xy}. The rest of the wandering electrons which collide with scatterers follow the conventional Drude expressions for conductivity. Taking into account the contributions of both types of electrons, the resultant longitudinal resistivity is given by [28]:

$$\rho_{xx} = \rho_0 \frac{1-P}{1+P^2/\beta^2} \qquad (2)$$

where ρ_0 is the zero-field resistivity, $P = \exp(-2\pi/\beta)$, $\beta = l_{tr}/R_c$ with l_{tr} being the transport mean free path, $R_c = v_F/\omega_c$ the cyclotron radius, and v_F the Fermi velocity. As shown in Fig.S3(b), Eq.2 predicts a much stronger field dependence of the NMRs than the experimentally observed one.

In real systems, a combination of different types of disorder such as background impurities, interface roughness, and dislocations can exist. After considering memory effects in a 2DEG with a random array of strong scatterers on the background of a smooth random potential remote impurities, Mirlin et. al. also obtained a negative parabolic correction to the magnetoresistance [29]:

$$\gamma_{\mathrm{MR}} \approx -(\omega_c/\omega_0)^2 \qquad (3)$$

where $\omega_0 = (2\pi N_s)^{1/2} v_F (2l_s/l_L)^{1/2}$, with N_s being the concentration of strong scatterers, and

l_s and l_L the mean free paths due to the scattering by strong and smooth potential scatterers, respectively.

Although Eq.3 can account for the observed parabolic relationship between the NMRs and the magnetic field as does Eq.1, this quasiclassical model predicts a temperature-independent NMR. At $T \leq 15$ K, NMRs in our samples are indeed temperature-insensitive. However, at $T > 15$ K the temperature suppresses the NMRs, as demonstrated in Fig.2(c) and Fig.S2(a). It is possible that both quantum (EEI) and quasiclassical effects contribute to the observed NMRs, resulting in the observed change of NMRs with temperature [10]. The upturn of the γ_{MR}s at high magnetic fields also indicates possible contributions by Zeeman splitting that can give rise to positive γ_{MR}s [2,25], which become more pronounced at higher temperatures. In fact, Cho et al. investigated NMRs of the 2DEG in an AlGaN/GaN heterostructure and concluded that quantum contribution and quasiclassical effects co-exist, with a dominance of the latter [19]. Cho et al. used the ratio of $\tau_{\mathrm{tr}}/\tau_{\mathrm{q}}$ to elucidate the type of strong scatterers that cause the quasiclassical NMRs, where τ_{tr} and τ_{q} are transport scattering time and the single particle relaxation time or quantum time, respectively. $\tau_{\mathrm{tr}}/\tau_{\mathrm{q}}$ is close to one for alloy or phonon scattering, while it could be significantly enhanced for scattering by interface roughness. They obtained a ratio of ~10 and attributed the interface roughness to be the strong scatterers.

Shubnikov–de Haas (SdH) quantum oscillations contain rich information of the 2DEG, i.e., the density of the charge carriers, their effective mass and quantum scattering time. Data in Fig.2 shows pronounced SdH quantum oscillations in our sample. Figure 3(a) presents the data after subtracting the background at temperatures between 3 K to 20 K, with the fast Fourier transform

(FFT) results shown in Fig.3(b). From the SdH oscillation frequency f = 214 T, we obtain the 2DEG density $n = 1.05\times10^{13}$ cm^{-2} from the relationship of $f = hn/2e$, where h is the Planck constant, and e is electron charge. This value is consistent with the electron density derived from the Hall measurements, as presented in Fig.1(d). The SdH oscillation frequency shows no sub-bands, indicating that only one type of charge carrier is present in our sample, i.e., the sample is of high quality.

The SdH oscillations can be used to derive the effective mass m^* and the quantum time τ_q through the Lifshitz-Kosevich formula [19]:

$$\frac{\Delta R}{R_0} = \frac{4X}{sinhX}\exp\left(-\frac{\pi}{\omega_c\tau_q}\right)cos\left(\frac{2\pi^2\hbar n}{eB}\right) \qquad (4)$$

where ΔR is the SdH oscillation component of the resistance (see Fig.3(a)), $X = 2\pi^2 k_B T/\hbar\omega_c$, k_B is Boltzmann constant and $\hbar$ is the reduced Planck constant. Since the cyclotron frequency $\omega_c = eB/m^*$, the effective mass m^* can be derived from the temperature dependence of ΔR at a fixed magnetic field. We chose ΔR_M at B = 11.46 T corresponding to the largest positive peak in the SdH oscillations and plot them in Fig.3(c). A curve fit with Eq.4 gives $m^* = 0.1975m_0$, with m_0 being the free electron mass. From the mobility μ values in Fig.1(d) and the relationship $\mu = e\tau_{tr}/m^*$, we obtain the transport scattering time $\tau_{tr} \approx 0.73$ ps. For a fixed temperature, we can simplify Eq.4 to $ln\left(\frac{\Delta R_M sinhX}{4R_0X}\right) \approx -\frac{\pi m^*}{Be\tau_q}$ to derive the quantum time τ_q, where ΔR_M represents the peak values at magnetic fields where $cos\left(\frac{2\pi^2\hbar n}{eB}\right) = 1$. Figure 3(d) presents the experimental results of $ln\left(\frac{\Delta R_M sinhX}{4R_0X}\right) \sim -1/B$ for T = 3 K. The slope gives a quantum time of τ_q = 0.078 ps, resulting in a ratio of $\tau_{tr}/\tau_q \approx 9.2$.

The determined ratio of τ_{tr}/τ_q in our sample is very close to the value of 10 obtained by Cho et al for an AlGaN/GaN heterostructure [19]. However, the quantum time τ_q deduced from the analysis of the SdH oscillations is much smaller than the quantum scattering time τ_{CR} determined from the width of the cyclotron resonance peak in the presence of small macroscopic inhomogeneity [48]. EEI experiments also reveal τ_{tr}/τ_q of 4~20 for long-range scattering by background impurity [2]. Thus, it is debatable if the ratio of τ_{tr}/τ_q can provide a reliable way to determine the scattering mechanism [19,48]. In order to directly uncover the scattering mechanisms responsible for the observed NMRs, we conducted electric field gating experiments to determine the mobility versus electron density relationship, which is strongly correlated with the various scattering mechanisms and can be quantitatively analyzed [32,33].

Figure 4(a) shows the dependence of sample resistances on the gate voltage V_g at B = 0 T and 12 T. As expected, the curve for B = 0 T is smooth while that for B = 12 T depicts oscillations due to gating-induced change in the electron density which varies the Fermi level, resulting in SdH quantum oscillations in a fixed magnetic field. In Fig.5(a) we present the relationship between the electron density determined using Hall measurements and the gate voltage. The electron density increases linearly with the gate voltage up to V_g = 1 V and further increases but at a slower rate beyond V_g > 1 V (sample W2 shows a linear relationship between the density and gate voltage at V_g < 2 V and a slight density decrease at V_g > 2.3 V, as presented in Fig.S5). This can be attributed to hole injection from the gate at high positive gating voltage [49]. By systematically measuring $R(V_g)$ curves at various magnetic fields and using the Hall electron density, we could construct a γ_{MR} color map as presented in Fig.4(b). The SdH oscillations induced Landau fan diagram can be

clearly seen.

Figure 4(a) also shows that the resistances do not change significantly beyond $V_g \geq -2$ V while increasing quickly when V_g becomes more negative at $V_g < -2$ V. More importantly, the resistances at $B = 12$ T, when the SdH oscillations are neglected, can be larger than those at $B = 0$ T at very negative V_g. Inset of Fig.4(a) shows γ_{MR} versus B curves at three values of V_g. Clearly, the NMRs are stronger at $V_g = 0$ V, in comparison to those at $V_g = -4$ V (in fields up to $B = 12$ T) and $V_g = 4$ V (in fields up to $B = 9$ T). It indicates that NMRs may only occur in a certain range of V_g (see Fig.S4 and Fig.S6 for similar effects in Sample W2). This can be further demonstrated by the *MR* versus V_g curves for various magnetic fields in Fig.5(b), where each curve shows a maximum in the amplitude of NMRs, though the corresponding V_g point shifts to more positive values with increasing magnetic field. That is, the amplitude of NMRs depends on the electron density. A more complete picture on the effects of electron density on the γ_{MR} can be seen from the color map in Fig.4(b), which shows more pronounced NMRs in the intermediate range of the electron density, i.e., 0.6×10^{13} cm^{-2} < n < 1.1×10^{13} cm^{-2}.

As pointed out above, it is the mobility versus density relationship rather the density itself that can provide information on the scattering mechanisms. Figure 5(a) presents the mobilities obtained at various gate voltages. The $\mu(V_g)$ curve exhibits a bell shape. The mobility increases rapidly with V_g first, reaches a maximal value of 12186 cm^{2}V^{-1}s^{-1} at $V_g = -2.8$ V and then decreases slowly with a further increase in V_g.

As shown in Fig.5(a), the electron density n does not follow a linear dependence on the gate voltage at high positive V_g. We plot the experimental $\mu(n)$ data in Fig.6. Theoretically, the

relationship between mobility and density is determined by the types of possibly co-existing scatterers such as background impurities, interface roughness, dislocations, and alloy disorder. Their scattering contributions are independent of each other and the total mobility can be calculated according to Matheissen's rule by combining different scattering mechanisms [35,46]. Experimentally, the density dependence of the electron mobility in AlGaN/GaN heterostructures has been systematically studied and found to follow the theory very well [33]. Details of the calculations, including the relevant equations and parameters are presented in the supplement [45]. Figure 6 shows a comparison of our experimental data with the calculated $\mu(n)$ curve as well as the individual contributions of background impurities, interface roughness, dislocations and alloy disorder. For simplicity we did not include the contribution from phonon scattering that is negligible at low temperatures. The results show that at low densities the electron scattering due to background impurity and dislocations limit the electron mobility, which becomes higher with increasing density. The downturn of the $\mu(n)$ curve at high electron densities is an indication of a cross-over to scattering by interface roughness, which is more than two orders of magnitude stronger than alloy scattering. The negligible influence of alloy scattering on total mobility is expected due to the intentionally introduced AlN barrier [25,44]. Together with the results in Fig.5, which shows that NMRs occur in the right side of the bell-shaped $\mu(V_g)$ curve and tend to vanish quickly in the left side, we can conclude that interface roughness is the key contributor to the NMRs observed in our samples.

As discussed above, strong scatterers alone could only induce NMR behavior described by Lorentz gas model Eq.2. The varnishing of NMRs in the left side of the bell-shaped $\mu(V_g)$ curve in

Fig.5 where scattering of smooth random potential dominates can also exclude the EEI mechanism that gives Eq.1 as the origin of the observed NMRs. On the other hand, Eq.3 can correctly explain the parabolic behavior as shown in Fig.2. Fig.6 also shows the presence of both strong scatterers and smooth random potential. Thus, we can safely attribute the observed NMRs to memory effects. This is in fact consistent with the results in Figs.4(b), Fig.5(b) and Fig.6, which reveal that NMRs are more pronounced when the scatterings from interface roughness and background impurity are comparable. They diminish quickly when the contribution of interface roughness is weaker than that from dislocations. On the other hand, the amplitude of the NMR also becomes smaller when the effect of background impurity is reduced at high electron density.

IV. CONCLUSION

In summary, we investigated the magnetoresistance behavior of 2DEGs in AlGaN/GaN heterostructures. Large NMRs were observed in a wide range of temperature. Analysis of the magnetic field and temperature dependences of the NMRs as well as the ratio of transport scattering time and quantum time suggest that the observed NMRs most likely originate from memory effects, with interface roughness to be the strong scatterers. We also conducted electric field gating experiments to obtain the electron mobility and density relationship that helps to further uncover the underlying scattering sources in the sample. The results confirmed the crucial role of interface roughness scattering in the occurrence of NMRs and also demonstrated that electric field gating can be a useful means in uncovering the various mechanisms for NMRs.

ACKNOWLEDGMENTS

This work is supported by the National Key R&D Program of China (2018YFA0209002), the National Natural Science Foundation of China (61771235, 61971464, 61727805, 11961141002, 61974113, 62074077,61921005, 61674080, and 61974060), Jiangsu Excellent Young Scholar Program (BK20200008) and Jiangsu Shuangchuang Program. W. K. Kwok is supported by the U.S. Department of Energy, Office of Science, Basic Energy Sciences, Materials Sciences and Engineering. Z.-L.X. acknowledges supports by the National Science Foundation under Grant No. DMR-1901843.

*Correspondence to: xiao@anl.gov; yongleiwang@nju.edu.cn; xllu@xidian.edu.cn

References

[1] M.A. Paalanen, D.C. Tsui, and J. C.M. Hwang, Parabolic magnetoresistance from the interaction effect in a two-dimensional electron gas, Phys. Rev. Lett. **51**, 2226 (1983).

[2] L. Li, Y. Y. Proskuryakov, A. K. Savchenko, E. H. Linfield, and D. A. Ritchie, Magnetoresistance of a 2D electron gas caused by electron interactions in the transition from the diffusive to the ballistic regime, Phys. Rev. Lett. **90**, 076802 (2003).

[3] L. Bockhorn, P. Barthold, D. Schuh, W. Wegscheider, and R. J. Haug, Magnetoresistance in a high-mobility two-dimensional electron gas, Phys. Rev. B **83**, 113301 (2011).

[4] A. T. Hatke, M. A. Zudov, J. L. Reno, L. N. Pfeiffer, and K. W. West, Giant negative magnetoresistance in high-mobility two-dimensional electron systems, Phys. Rev. B **85**, 081304(R) (2012).

[5] R. G. Mani, A. Kriisa, and W. Wegscheider, Size-dependent giant-magnetoresistance in millimeter scale GaAs/AlGaAs 2D electron devices, Sci. Rep. **3**, 2747 (2013).

[6] L. Bockhorn, I. V. Gornyi, D. Schuh, C. Reichl, W. Wegscheider, and R. J. Haug, Magnetoresistance induced by rare strong scatterers in a high-mobility two-dimensional electron gas, Phys. Rev. B **90**, 165434 (2014).

[7] Q. Shi, M. A. Zudov, L. N. Pfeiffer, and K. W. West, Nonlinear transport in two-dimensional electron gas exhibiting colossal negative magnetoresistance, Phys. Rev. B **90**, 201301(R) (2014).

[8] Q. Shi, P. D. Martin, Q. A. Ebner, M. A. Zudov, L. N. Pfeiffer, and K.W. West, Colossal negative magnetoresistance in a two-dimensional electron gas, Phys. Rev. B **89**, 201301 (2014).

[9] J. Iñarrea, L. Bockhorn, and R. J. Haug, Negative huge magnetoresistance in high-mobility 2D electron gases: DC-current dependence, Europhys. Lett. **115**, 17005 (2016).

[10] J. Kanter, S. Vitkalov, and A. A. Bykov, Anomalous negative magnetoresistance of two-dimensional electrons, Phys. Rev. B **97**, 205440 (2018).

[11] N. H. Siboni, J. Schluck, K. Pierz, H.W. Schumacher, D. Kazazis, J. Horbach, and T. Heinzel, Nonmonotonic classical magnetoconductivity of a two-dimensional electron gas in a disordered array of obstacles, Phys. Rev. Lett. **120**, 056601 (2018).

[12] J. Schluck, M. Hund, T. Heckenthaler, and T. Heinzel, N. H. Siboni and J. Horbach, K. Pierz, H. W. Schumacher, D. Kazazis, U. Gennser, and D. Mailly, Linear negative magnetoresistance in two-dimensional Lorentz gases, Phys. Rev. B **97**, 115301 (2018).

[13] R. L. Samaraweera, H.-C. Liu, B. Gunawardana, A. Kriisa, C. Reichl, W. Wegscheider, and R. G. Mani, Sci. Rep. **8**, 10061 (2018).

[14] R. L. Samaraweera, B. Gunawardana, T. R. Nanayakkara, R. C. Munasinghe, A. Kriisa, C. Reichl, W. Wegscheider, and R. G. Mani, Coherent backscattering in quasi-ballistic ultra-high mobility GaAs/AlGaAs 2DES, Sci. Rep. **10**, 781 (2020).

[15] A. Buyanov, J. Bergman, J. Sandberg, B. Sernelius, P. Holtz, B. Monemar, H. Amano, and I. Akasaki, Influence of potential fluctuations on electrical transport and optical properties in modulation-doped GaN/$Al_{0.28}Ga_{0.72}N$ heterostructures, Phys. Rev. B **58**, 1442 (1998).

[16] A. V. Buyanov, J. A. Sandberg, B. E. Sernelius, P. O. Holtz, J. P. Bergman, B. Monemar, H. Amano, and I. Akasaki, Weakly localized transport in modulation-doped GaN/AlGaN heterostructures, J. Cryst. Growth **189/190**, 758 (1998).

[17] J. Antoszewski, M. Gracey, J. M. Dell, L. Faraone, T. A. Fisher, G. Parish, Y.-F. Wu, and U. K. Mishra, Scattering mechanisms limiting two-dimensional electron gas mobility in $Al_{0.25}Ga_{0.75}N$/GaN modulation-doped field-effect transistors, J. Appl. Phys. **87**, 3900 (2000).

[18] A. F. Braña, C. Diaz-Paniagua, F. Batallan, J. A. Garrido, E. Muñoz, and F. Omnes, Scattering times in AlGaN/GaN two-dimensional electron gas from magnetoresistance measurements, J. Appl. Phys. **88**, 932 (2000).

[19] H. I. Cho, G. M. Gusev, Z. D. Kvon, V. T. Renard, J. H. Lee, and J. C. Portal, Negative quasiclassical magnetoresistance in a high density two-dimensional electron gas in a $Al_xGa_{1-x}N$/GaN heterostructure, Phys. Rev. B **71**, 245323 (2005).

[20] J. Xu, M. K. Ma, M. Sultanov, Z. -L. Xiao, Y. -L. Wang, D. Jin, Y. -Y. Lyu, W. Zhang, L. N. Pfeiffer, K. W. West, K. W. Baldwin, M. Shayegan, and W. -K. Kwok, Negative longitudinal magnetoresistance in gallium arsenide quantum wells, Nat. Commun. **10**, 287 (2019).

[21] Y.-Y. Lyu, X. -J. Zhou, Z. -L. Xiao, R. Fotovat, J. Xu, G. Basnet, Y. -L. Wang, D. Jin, R. Divan, H. -B. Wang, and W. -K. Kwok, Non-Ohmic negative longitudinal magnetoresistance in a two-dimensional electron gas, Phys. Rev. B **103**, 035422 (2021).

[22] M. K. Mishra, R. K. Sharma, R Tyagi, R Manchanda, A. K. Pandey, O. P. Thakur, and R Muralidharan, Large negative magnetoresistance induced by interplay between smooth disorder and antidots in AlGaN/GaN HEMT structures, Mater. Res. Express **3**, 045902 (2016).

[23] K. H. Gao, X. R. Ma, D. B. Zhou, S. Li, Z. Q. Li, T. Lin, X. H. Zhang, and W. Z. Zhou, Magnetotransport property of graded AlGaN/GaN heterostructure, Superlattices and Microstructures **135**, 106262 (2019).

[24] B. L. Altshuler, D. Khmelnitski, A. I. Larkin, and P. A. Lee, Magnetoresistance and Hall effect in a disordered two-dimensional electron gas, Phys. Rev. B **22**, 5142 (1980).

[25] B. L. Altshuler and A. G. Aronov, Electron-Electron Interaction in Disordered Systems, edited by A.L. Efros and M. Pollak (North-Holland, Amsterdam, 1985).

[26] I. V. Gornyi and A. D. Mirlin, Interaction-induced magnetoresistance: From the diffusive to the ballistic regime, Phys. Rev. Lett. **90**, 076801 (2003).

[27] A. Dmitriev, M. Dyakonov, and R. Jullien, Anomalous low-field classical magnetoresistance in two dimensions, Phys. Rev. Lett. **89**, 266804 (2002).

[28] A. Dmitriev, M. Dyakonov, and R. Jullien, Classical mechanism for negative magnetoresistance in two dimensions, Phys. Rev. B **64**, 233321 (2001).

[29] A. D. Mirlin, D. G. Polyakov, F. Evers, and P. Wölfle, Quasiclassical negative magnetoresistance of a 2D electron gas: Interplay of strong scatterers and smooth disorder, Phys. Rev. Lett. **87**, 126805 (2001).

[30] V. K. Dugaev, M. Inglot, E. Y. Sherman, J. Berakdar, and J. Barnas, Nonlinear anomalous Hall effect and negative magnetoresistance in a system with random Rashba field, Phys. Rev. Lett. **109**, 206601 (2012).

[31] P. S. Alekseev, Negative magnetoresistance in viscous flow of two-dimensional electrons, Phys. Rev. Lett. **117**, 166601 (2016).

[32] J. L. Farvacque and Z. Bougrioua, Carrier mobility versus carrier density in $Al_xGa_{1-x}N$/GaN quantum wells, Phys. Rev. B 68, 035335 (2003).

[33] P. Lorenzini, Z. Bougrioua, A. Tiberj, R. Tauk, M. Azize, M. Sakowicz, K. Karpierz, and W. Knap, Quantum and transport lifetimes of two-dimensional electrons gas in AlGaN/GaN heterostructures, Appl. Phys. Lett. **87**, 232107 (2005).

[34] D. Laroche, S. Das Sarma, G. Gervais, M. P. Lilly, and J. L. Reno, Scattering mechanism in modulation-doped shallow two-dimensional electron gases, Appl. Phys. Lett. **96**, 162112 (2010).

[35] B. Shojaei, A. C. C. Drachmann, M. Pendharkar, D. J. Pennachio, M. P. Echlin, P. G. Callahan, S. Kraemer, T. M. Pollock, C. M. Marcus, and C. J. Palmstrøm, Limits to mobility in InAs quantum wells with nearly lattice-matched barriers, Phys. Rev. B **94**, 245306

(2016).

[36] Y. F. Wu, D. Kapolnek, J. P. Ibbetson, P. Parikh, B. P. Keller, and U. K. Mishra, An insulator-lined silicon substrate-via technology with high aspect ratio, IEEE Trans. Electron Devices **48**, 586 (2001).

[37] R. S. Pengelly, S. M. Wood, J. W. Milligan, S. T. Sheppard, and W. L. Pribble, A review of GaN on SiC high electron-mobility power transistors and MMICs, IEEE Trans. Microwave Theory Technol. **60**, 1764 (2012).

[38] H. Otake, K. Chikamatsu, A. Yamaguchi, T. Fujishima, and H. Ohta, Vertical GaN-based trench gate metal oxide semiconductor field-effect transistors on GaN bulk substrates, Appl. Phys. Express **1**, 011105 (2008).

[39] B. Rau, P. Waltereit, O. Brandt, M. Ramsteiner, K. H. Ploog, J. Puls, and F. Henneberger, In-plane polarization anisotropy of the spontaneous emission of *M*-plane GaN/(Al,Ga)N quantum wells, Appl. Phys. Lett. **77**, 3343 (2000).

[40] E. Kuokstis, C. Q. Chen, M. E. Gaevski, W. H. Sun, J. W. Yang, G. Simin, M. Asif Khan, H. P. Maruska, D. W. Hill, M. C. Chou, J. J. Gallagher, and B. Chai, Polarization effects in photoluminescence of *C*- and *M*-plane GaN/AlGaN multiple quantum wells, Appl. Phys. Lett. **81**, 4130 (2002).

[41] O. Ambacher, J. Smart, J. R. Shealy, N. G. Weimann, K. Chu, M. Murphy, W. J. Schaff, and L. F. Eastman, Two-dimensional electron gases induced by spontaneous and piezoelectric polarization charges in N- and Ga-face AlGaN/GaN heterostructures, J. Appl. Phys. **85**, 3222 (1999).

[42] See Supplemental Material at http://link.aps.org/supplemental/ 10.1103/PhysRevMaterials.XX.XXXXXX be inserted by publisher] for the calculation of mobility versus density relationship, a comparison of the temperature dependence of the electron density, mobility, and mean free path as well as the electron mobility versus density relationship from CH1 and CH2 of Sample W1, and for additional data from CH2 of Sample W1 and Sample W2.

[43] R. K. Jana and D. Jena, Stark-effect scattering in rough quantum wells, Appl. Phys. Lett. **99**, 012104 (2011).

[44] Q. Li, J. Zhang, L. Meng, J. Chong, and X. Hou, Mobility limitations due to dislocations and interface roughness in AlGaN/AlN/GaN heterostructure, J. Nanomater. **2015**, 903098 (2015).

[45] L. Hsu and W. Walukiewicz, Effect of polarization fields on transport properties in AlGaN/GaN heterostructures, J. Appl. Phys. **89**, 1783 (2001).

[46] D. Jena, Y. Smorchkova, C. Elsass, A. C. Gossard, and U. K. Mishra: Electron transport and intrinsic mobility limits in two-dimensional electron gases of III–V nitride heterostructures. arXiv:cond-mat/0103461 (2001).

[47] N. Tang, B. Shen, K. Han, F. C. Lu, Z. X. Qin and G. Y. Zhang, Abnormal Shubnikov–de Haas oscillations of the two-dimensional electron gas in $Al_xGa_{1-x}N/GaN$ heterostructures in tilted magnetic fields, Phys. Rev. B **79**, 073304 (2009).

[48] S. Syed, M. J. Manfra, Y. J. Wang, R. J. Molnar, and H. L. Stormer, Electron scattering in AlGaN/GaN structures, Appl. Phys. Lett. **84**, 1507 (2004).

[49] M. Meneghini, M. Scamperle, M. Pavesi, M. Manfredi, T. Ueda, H. Ishida, T. Tanaka, D. Ueda, G. Meneghesso, and E. Zanoni, Electron and hole-related luminescence processes in gate injection transistors, Appl. Phys. Lett. **97**, 033506 (2010)**.**

Figure captions

Fig.1. (a) Schematic (not-to-scale) of the layer structuring of the AlGaN/GaN heterostructure. (b) Micrograph and enlarged view of the sample in Hall bar geometry with width of L_y = 200 μm and voltage lead distance of L_x = 250 μm. CH1 And CH2 in the enlarged view denote the measured Hall bar sections. Each section has four voltage contacts, with one pair in the longitudinal direction for measuring R_{xx} and one pair in the transverse direction for measuring R_{xy}. (c) Temperature dependence of the sample resistance in the absence of a magnetic field and the Hall resistance at B = 9 T. Inset shows the linear field dependence of the Hall resistances at the lowest (T = 3 K) and highest (T = 260 K) experimental temperatures. (d) Temperature dependence of the electron density n and mobility μ derived from data in (c).

Fig.2. (a) The magnetoresistance γ_{MR} at T = 3 K. The inset is an expanded view to show the weak localization induced cusp at zero-field. (b) Data in (a) plotted as γ_{MR} versus B^2 to show the parabolic field dependence. The main panel shows the linear section while the inset present the complete set of data. (c) Magnetoresistances $\gamma_{\mathrm{MR}}\, s$ obtained at various temperatures. The magnetic field is applied perpendicular to the 2DEG.

Fig.3. (a) Magnetic field dependence of the resistance components ΔR induced by Shubnikov–de

Haas (SdH) quantum oscillations at various temperatures. (b) Fast Fourier transform (FFT) spectra of the data in (a). (c) Temperature dependence of ΔR_M at B = 11.46 T (positive maxima in the SdH oscillations). Circles are experimental data and the line is a fit to Eq.4 to derive the effective mass m^*. (d) Magnetic field dependence of peak values ΔR_M in the SdH oscillations at T = 3 K. Circles are experimental data and the line is a fit to derive the quantum time from Eq.4.

Fig.4. (a) Gate voltage dependence of the sample resistance at B = 0 T and 12 T. The inset presents γ_{MR} versus B curves obtained at various gate voltages. (b) Color map of the field and electron density dependences of the magnetoresistance γ_{MR}. It is constructed by taking R ~ Vg curves at magnetic fields from 0 T to 4.5 T in intervals of 0.5 T and from 4.5 T to 12 T in intervals of 0.25 T. The data were taken at T = 3 K.

Fig.5. Gate voltage dependence of the electron mobility and density (a) and magnetoresistance γ_{MR} (b). The electron density is calculated from the measured Hall resistance. The mobility is derived from the measured zero-field resistance and the calculated Hall electron density. The data were taken at T = 3 K.

Fig.6. Comparison of the experimental and theoretical relationships between the electron mobility and density. Symbols are for experimental data and curves are calculated (Equations and discussions are presented in the supplement).

Figure 1

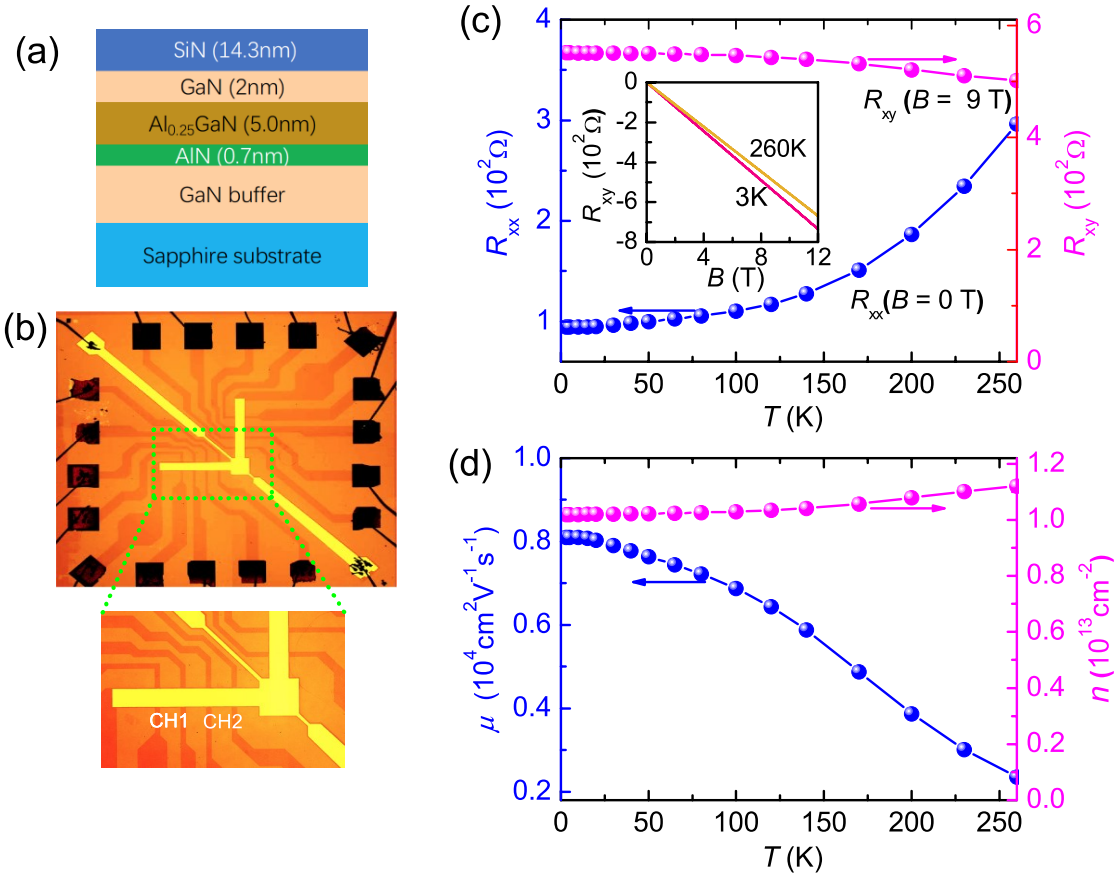
(a)
SiN (14.3nm)
GaN (2nm)
Al0.25GaN (5.0nm)
AlN (0.7nm)
GaN buffer
Sapphire substrate
(b)
CH1 CH2
(c)
Rxx (10^2Ω)
Rxy (10^2Ω)
T (K)
Rxy (B = 9 T)
Rxx (B = 0 T)
260K
3K
B (T)
(d)
μ (10^4cm^2V^-1s^-1)
n (10^13cm^-2)
T (K)

Figure 2

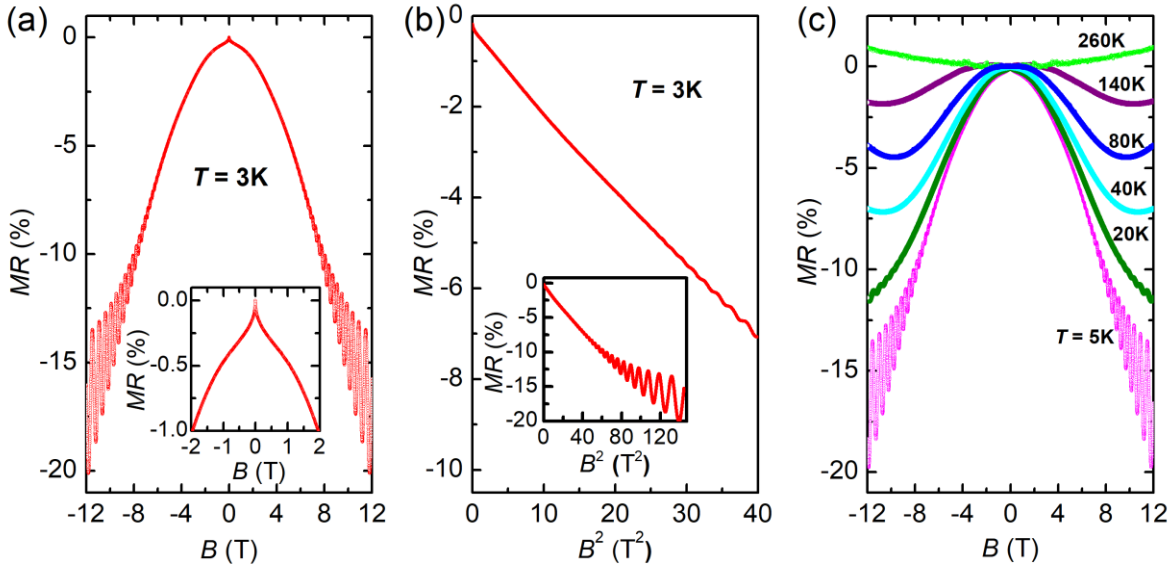

Figure 3

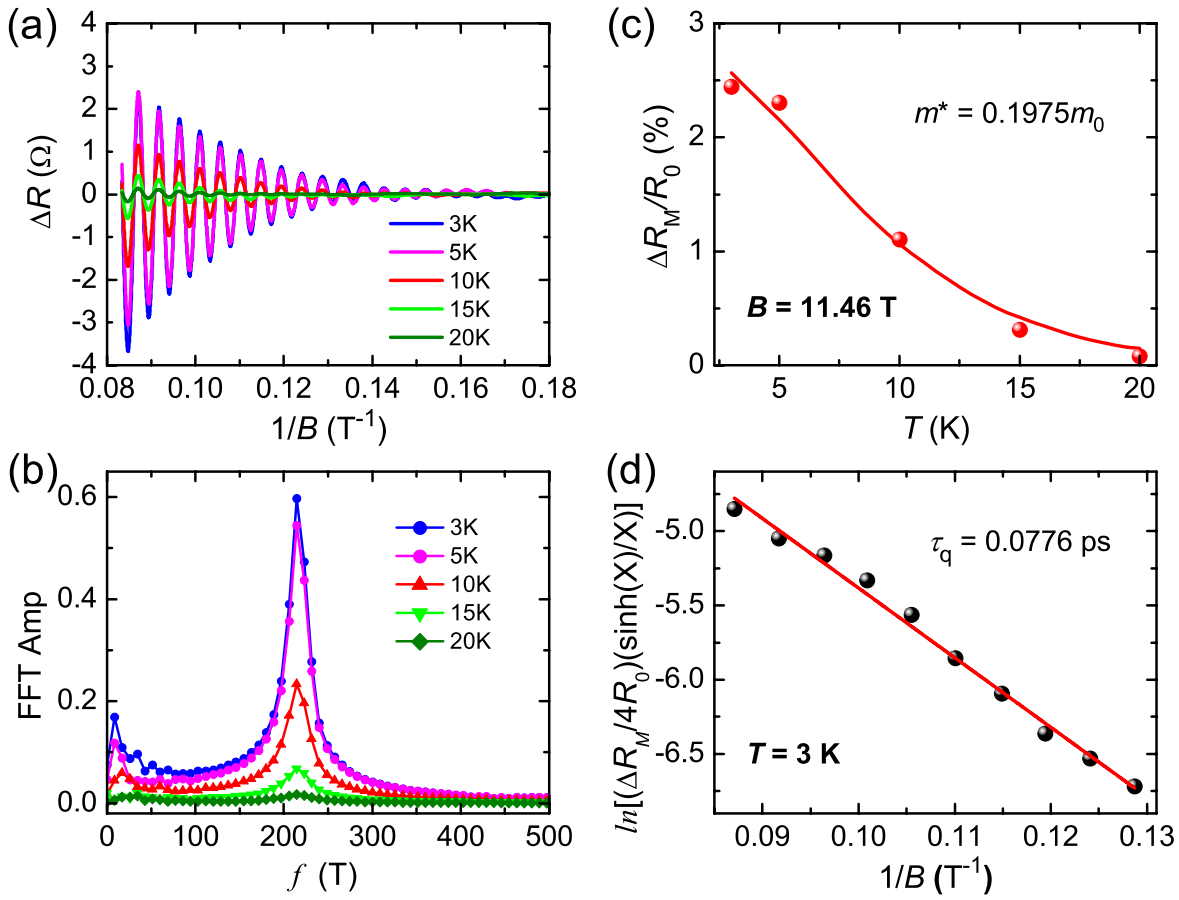
(a)
ΔR (Ω)
1/B (T^-1)
3K
5K
10K
15K
20K
(b)
FFT Amp
f (T)
3K
5K
10K
15K
20K
(c)
ΔR_M/R_0 (%)
m* = 0.1975m_0
B = 11.46 T
T (K)
(d)
ln[(ΔR_M/4R_0)(sinh(X)/X)]
τ_q = 0.0776 ps
T = 3 K
1/B (T^-1)

Figure 4

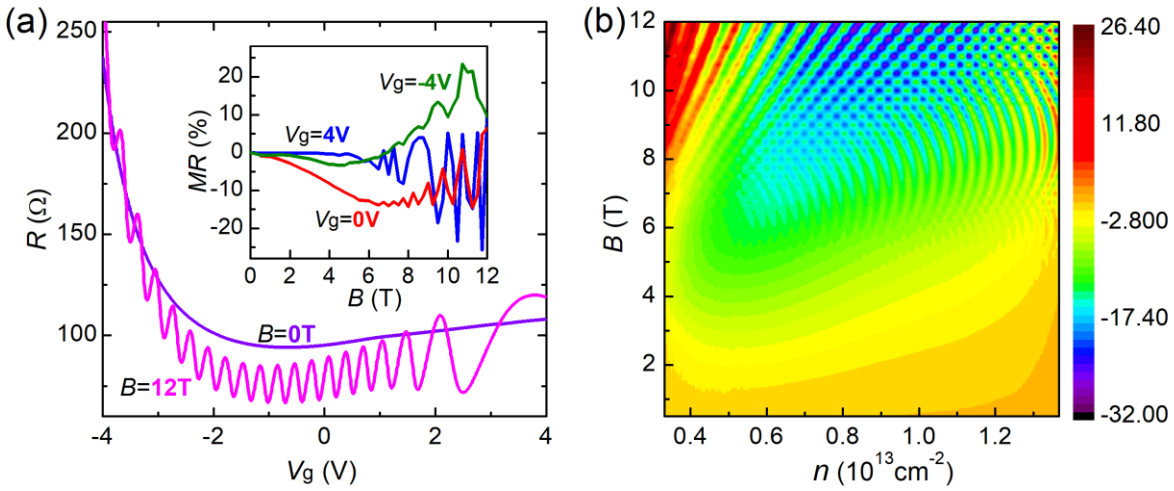
(a)
R (Ω)
Vg (V)
B=0T
B=12T
MR (%)
B (T)
Vg=-4V
Vg=4V
Vg=0V
(b)
B (T)
n (10^13 cm^-2)
26.40
11.80
-2.800
-17.40
-32.00

Figure 5

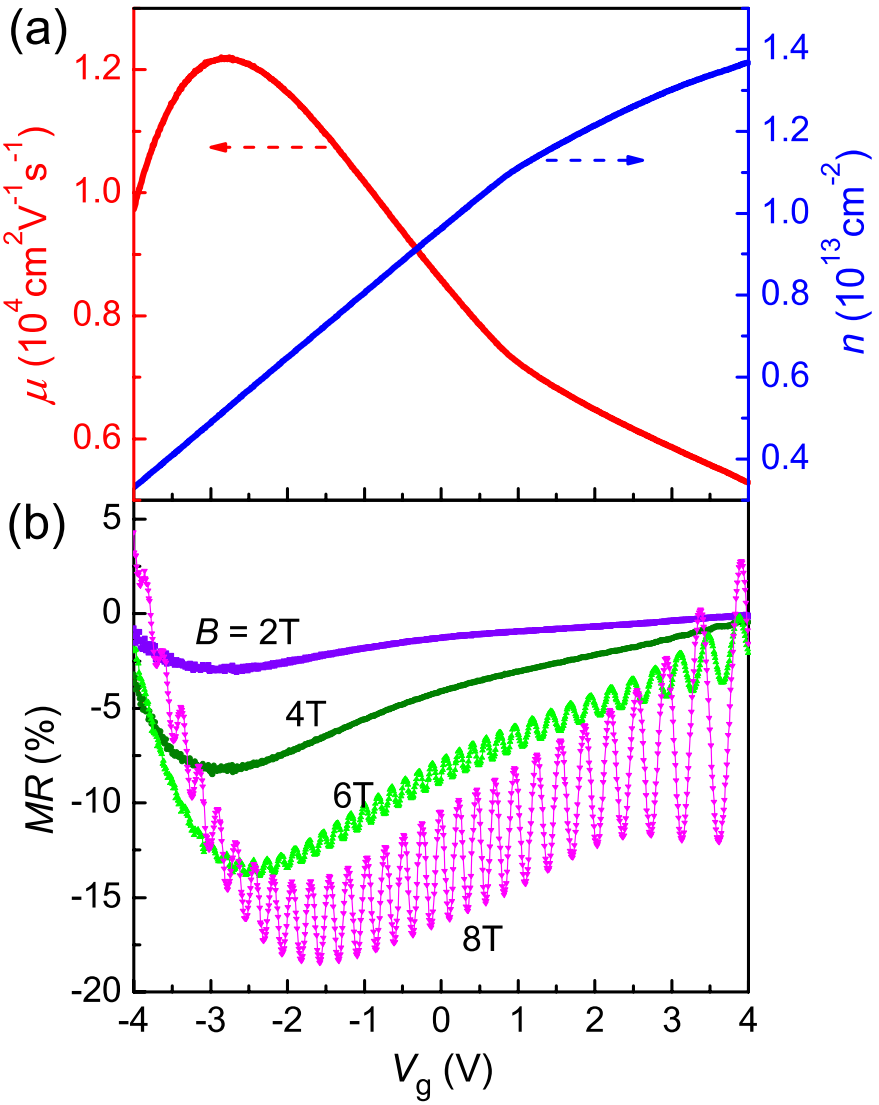
(a)
1.2
1.0
0.8
0.6
μ (10^4 cm^2 V^-1 s^-1)
1.4
1.2
1.0
0.8
0.6
0.4
n (10^13 cm^-2)
(b)
5
0
-5
-10
-15
-20
MR (%)
B = 2T
4T
6T
8T
-4
-3
-2
-1
0
1
2
3
4
V_g (V)

Figure 6

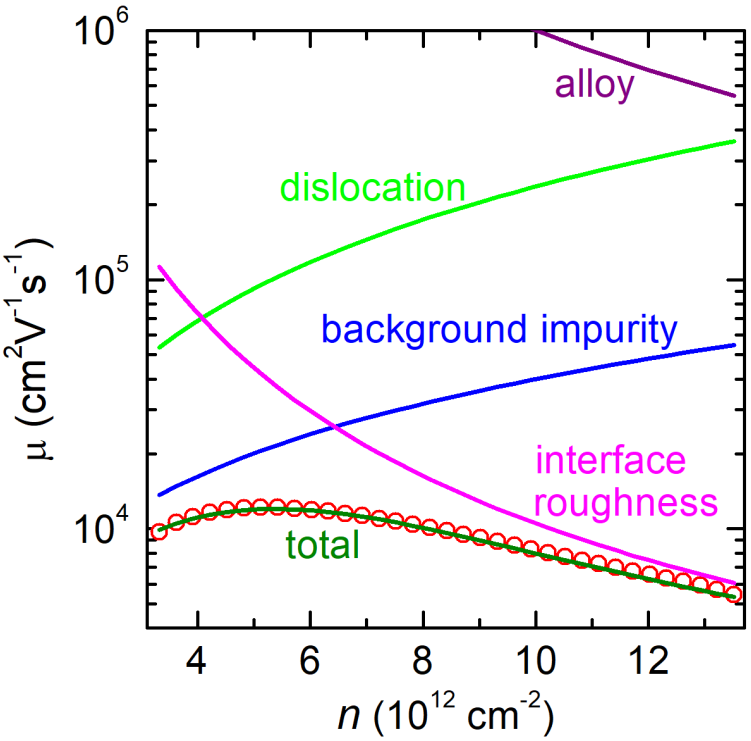
10^6
10^5
10^4
μ (cm^2V^-1s^-1)
alloy
dislocation
background impurity
interface
roughness
total
4
6
8
10
12
n (10^12 cm^-2)

Supplementary material

Interface roughness governed negative magnetoresistances in two-dimensional electron gases in AlGaN/GaN heterostructures

Ting-Ting Wang[1], Sining Dong[1], Zhi-Li Xiao[2,3,*], Chong Li[1], Wen-Cheng Yue[1], Bin-Xi Liang[1], Fei-Fan Xu[1], Yong-Lei Wang[1,*], Sheng-Rui Xu[4], Xiao-Li Lu[4,*], Jianhua Li[1], Chenguang Wang[1], Zixiong Yuan[1], Song-Lin Li[1], Guo-Zhu Sun[1], Bin Liu[1], Hai Lu[1], Hua-Bing Wang[1,5], and Wai-Kwong Kwok[2]

[1]*School of Electronic Science and Engineering, Nanjing University, Nanjing, 210023, China*

[2]*Materials Science Division, Argonne National Laboratory, Argonne, IL 60439, USA*

[3]*Department of Physics, Northern Illinois University, DeKalb, IL 60115, USA*

[4]*School of Microelectronics & State Key Discipline Laboratory of Wide Bandgap Semiconductor Technology, Xidian University, Xi'an, 710071, China*

[5]*Purple Mountain Laboratories, Nanjing, 211111, China*

Calculation of mobility versus density relationship

The relationship between mobility and density is determined by the types of possibly co-existed scatterers such as background impurities, interface roughness, dislocations, alloy disorder [1,2]. Their scattering contributions are independent of each other and the total mobility can be calculated according to Matheissen's rule by combining different scattering mechanisms, i.e., $\mu = e\tau/m^*$ and τ is calculated as follows [3,4]

$$\frac{1}{\tau} = \frac{1}{\tau_{back}} + \frac{1}{\tau_{IFR}} + \frac{1}{\tau_{dis}} + \frac{1}{\tau_{alloy}}$$

where τ_{back}, τ_{IFR}, τ_{dis}, and τ_{alloy} are the scattering times for the background impurities, interface roughness, dislocations, and alloy disorder, respectively.

The background impurities' scattering time τ_{back} is expressed as [4],

$$\frac{1}{\tau_{back}} = N_{back}\frac{m^*}{2\pi\hbar^3 k_F^3}\left(\frac{e^2}{2\epsilon}\right)^2 \int_0^{2k_F} dq \frac{1}{(q+q_{TF})^2}\frac{q}{\sqrt{1-(\frac{q}{2k_F})^2}}$$

where:

N_{back} is the background donor density,

$k_F = \sqrt{2\pi n}$ is the Fermi wave vector and n is the electron density,

$q_{TF} = 2/a_B^*$ is the Thomas-Fermi wave vector and reflects the screening length of 2DEG

a_B^* is the effective Bohr radius,

q is the difference of the wave vectors between the initial state and the final state in scattering.

The interface roughness scattering time τ_{IFR} is given as [5]

$$\frac{1}{\tau_{IFR}} = \left(\frac{e^2 n \Delta\Lambda}{2\varepsilon_s}\right)^2 \frac{m^*}{\hbar^3} J(k)$$

where

$$J(k) = \int_0^{2k} \frac{exp\,(-q^2\Lambda^2/4)}{2{k_F}^3(q+q_s)^2\sqrt{1-(q/2k_F)^2}} q^4 dq$$

Δ is root mean square roughness height and Λ is a correlation length. Here q_s is the screening constant, as

$$q_s = \frac{e^2 m^*}{2\pi\varepsilon_s\hbar^2}$$

The dislocation scattering is described as [4]

$$\frac{1}{\tau_{dis}} = N_{dis}\frac{m^*}{2\pi\hbar^3 k_F^3}\int_0^{2k_F} dq|V(q)|^2 \frac{q^2}{\sqrt{1-(\frac{q}{2k_F})^2}}$$

where N_{dis} is the 2D density of line dislocations and $V(q)$ is the screened potential,

$$V(q) = \frac{e\rho_L}{\epsilon}\frac{1}{q+q_{TF}}$$

the $\rho_L = ef/c_0$ is the dislocation line charge, where c_0 = 5.185 Å is the lattice constant in GaN along the (0001) direction and f is the fraction of occupied acceptor states introduced by the dislocation.

The alloy scattering time is quite sensitive to the electron density and can be expressed as $1/\tau_{alloy} = cn^2$ [6].

The calculation was done with the experimentally derived effective mass of $m^* = 0.1975m_0$ and the corresponding Bohr radius of a_B^* = 23.8 Å. The best fit to the experimental results produces a background density of $N_{back} = 2.5\times10^{17}$ cm^{-3}, dislocation density of $N_{dis} = 8\times10^8$ cm^{-2}, $f = 0.5$, interface roughness parameters $\Delta = 1.7$ Å, correlation length $\Lambda = 10$ Å and c = 10^{-36} cm^{2}s^{-1}. These parameters are consistent with those reported in the literature [1,2,4].

[1] J. L. Farvacque and Z. Bougrioua, Phys. Rev. B **68**, 035335 (2003).

[2] P. Lorenzini, Z. Bougrioua, A. Tiberj, R. Tauk, M. Azize, M. Sakowicz, K. Karpierz, and W. Knap, Appl. Phys. Lett. **87**, 232107 (2005).

[3] B. Shojaei, A. C. C. Drachmann, M. Pendharkar, D. J. Pennachio, M. P. Echlin, P. G. Callahan, S. Kraemer, T. M. Pollock, C. M. Marcus, and C. J. Palmstrøm, Phys. Rev. B **94**, 245306 (2016).

[4] D. Jena, Y. Smorchkova, C. Elsass, A. C. Gossard, and U. K. Mishra: Electron transport and intrinsic mobility limits in two-dimensional electron gases of III–V nitride heterostructures. arXiv:cond-mat/0103461 (2001).

[5] D. Zanato, S. Gokden, N. Balkan, B. K. Ridley, and W. J. Schaff, Semicond. Sci. Technol. **19**, 427 (2004).

[6] L. Hsu and W. Walikiewocz, Phys. Rev. B **56**, 1520 (1997).

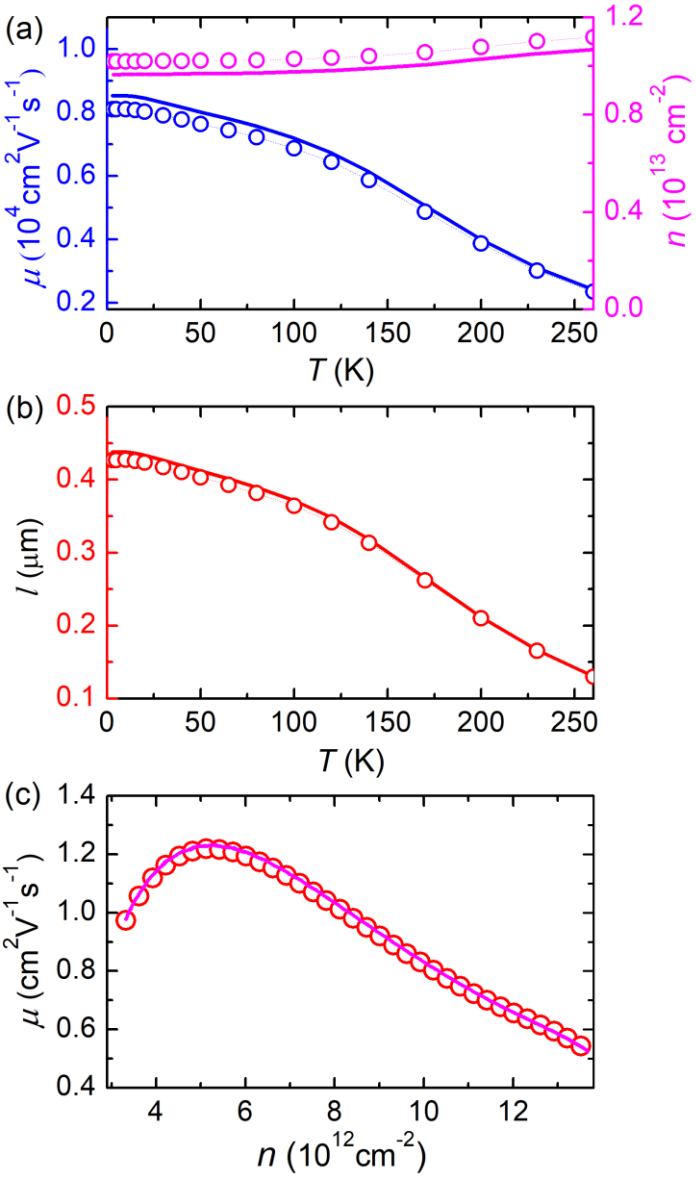

Fig.S1. Comparison of the results from CH1 and CH2 of Sample W1. (a) Temperature dependence of the electron density and mobility. (b) Temperature dependence of the electron mean free path. (c) Electron mobility versus density relationship. Symbols and thick solid lines are for CH1 and CH2, respectively. The results show the homogeneity of the sample.

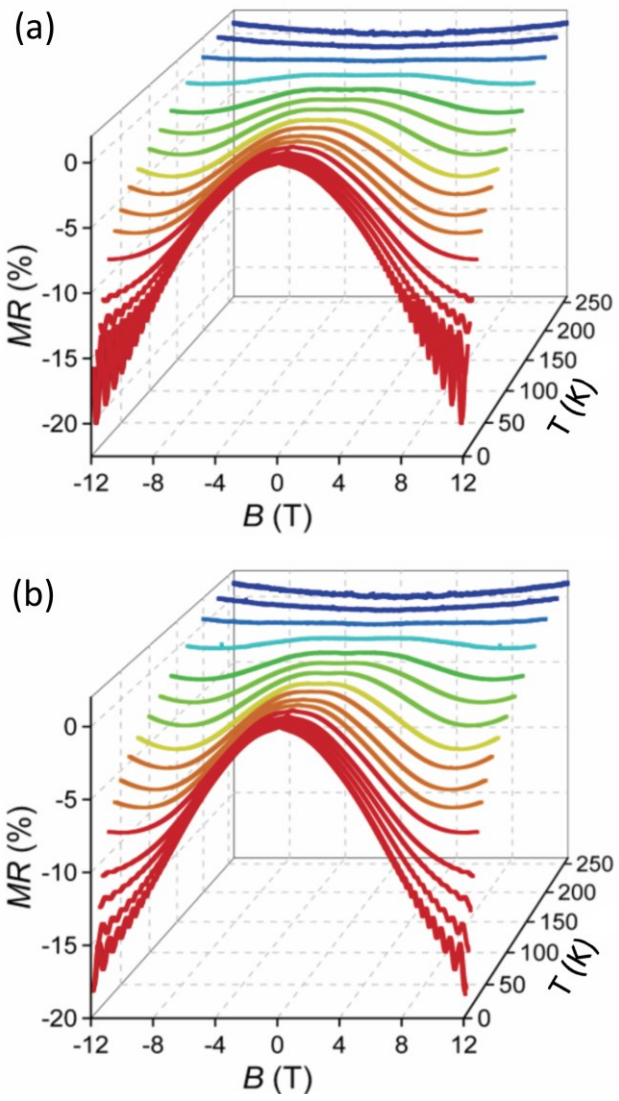

Fig.S2. Complete sets of magnetoresistances measured at temperatures between T = 3 K and T = 260 K. (a), and (b) are for CH1 and CH2 of Sample W1, respectively.

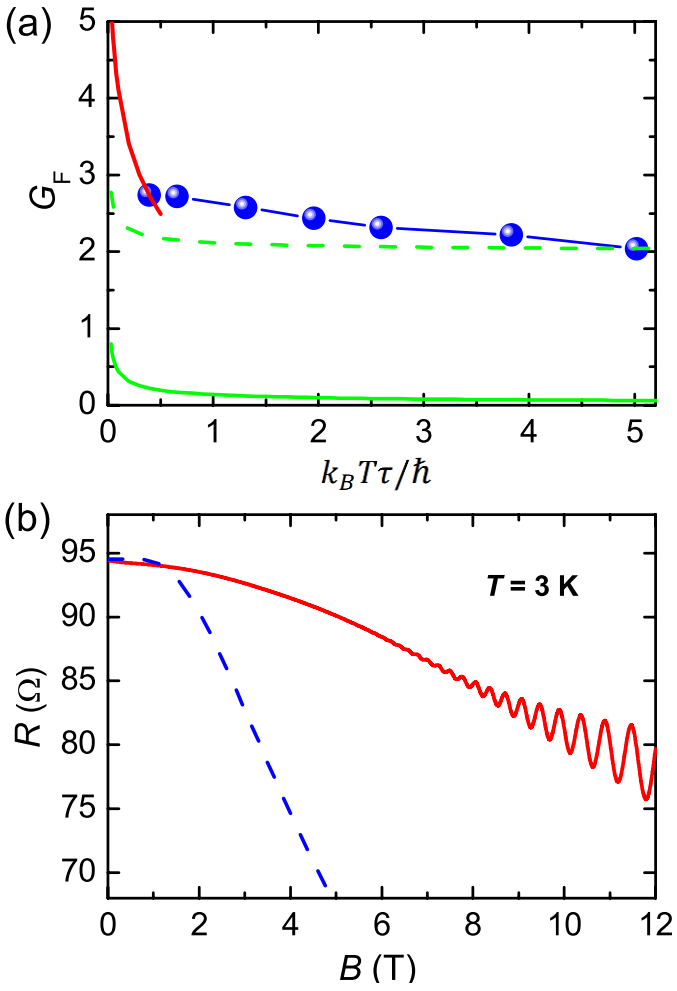

Fig.S3. Analysis results from various theories. (a) G_F versus $k_BT\tau/\hbar$ relationship derived from the EEI theory Eq.(1). Symbols are experimental data. Red and blue solid lines are theoretical curves $G_F \approx C - \ln(k_BT\tau/\hbar)$ with C is a constant and $G_F \approx (c_0/2)(k_BT\tau/\hbar)^{-1/2}$ with $c_0 \approx 0.276$ for $k_BT\tau/\hbar \ll 1$ and $k_BT\tau/\hbar > 1$, respectively. C = 1.8 was used in the calculation. The dashed green line represents a shift of the solid green by a constant of 1.98 along G_F so that the calculated G_F value is the same as the experimental one at $k_BT\tau/\hbar = 5$. The difference could indicate the relative contribution of the memory effect and the EEIs to the observed NMRs. (b) Magnetic field dependence of the resistance. Red solid line and blue dashed line are experimental results and a fit with the Lorentz gas model Eq.(2), respectively.

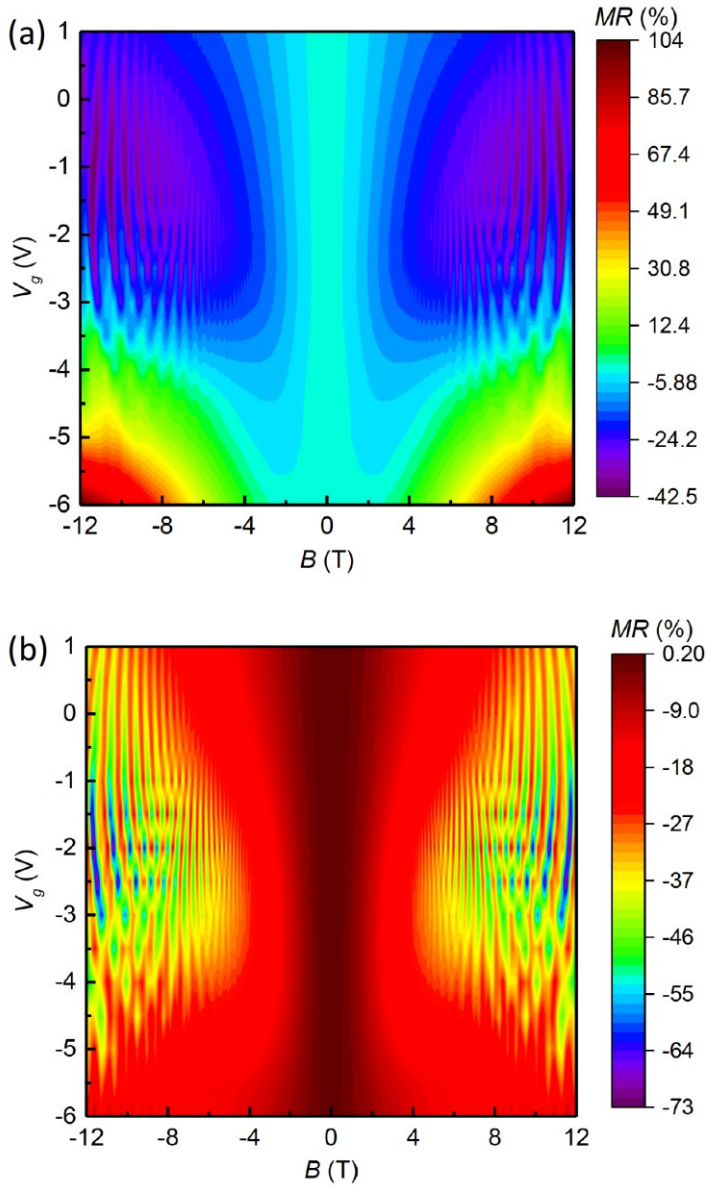

Fig.S4. Additional data on gate effects on the magnetoresistance. (a), and (b) are for CH1 and CH2 of Sample W2, respectively. Data were taken at T = 3 K. They show that magnetoresistance become positive at high negative gate voltages and NMRs are most pronounced in certain range of the gate voltage, consistent with the observation in Fig.4(b) and Fig.5(b) for CH1 of Sample W1.

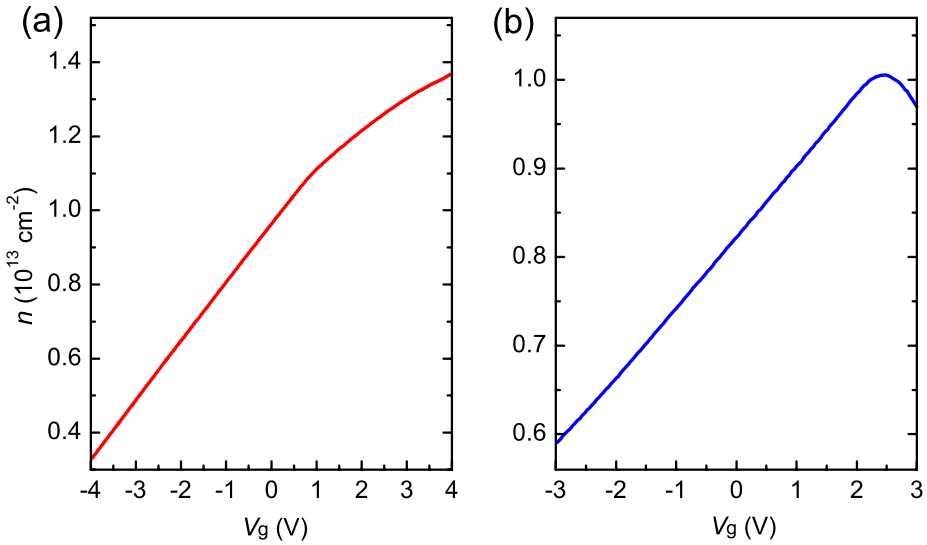

Fig.S5. Electron density versus gate voltage relationship. (a) CH2 of sample W1. (b) (a). CH1 of sample W2. The electron density is calculated from Hall resistance. The data were taken at $T = 3$ K. (a) shows nearly the same result as that in Fig.5(a), indicating the same behavior of different sections on the same sample. The difference in (a) and (b) reveals that electron density versus gate voltage relationship can differ from sample to sample, depending on factors such as the thickness of the insulating layer between the gate metallic layer and the 2DEG layer as well as he electron density in the absence of the gate voltage.

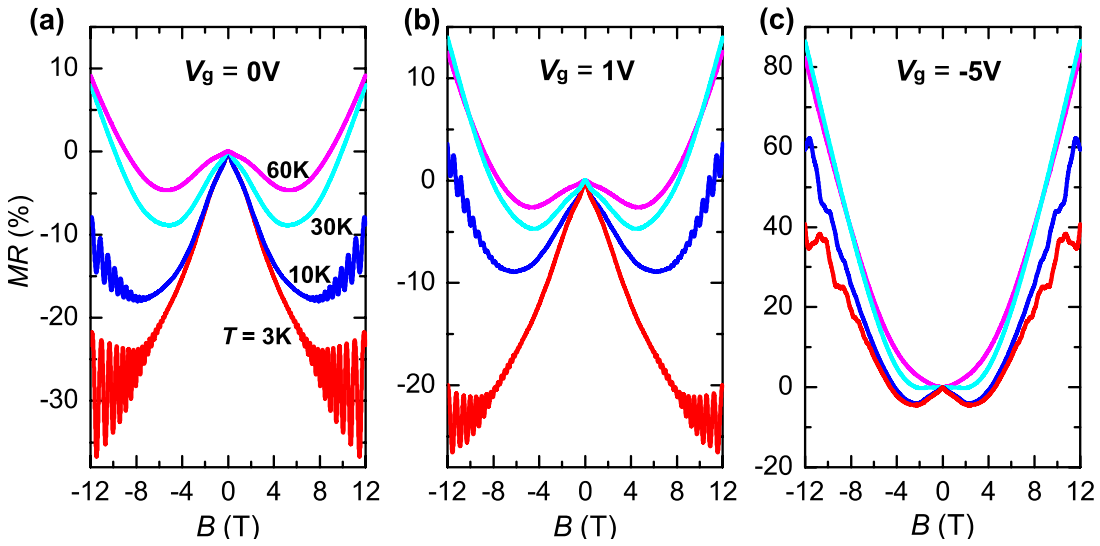

Fig.S6. Comparison of $MR(B)$ curves at various gate voltages. (a) $V_g = 0$ V. (b) $V_g = 1$ V. and (c) $V_g = -5$ V. The data were taken at $T = 3$ K (red curve), 10 K (blue curve), 30 K (cyan curve) and 60 K (magenta curve).